

Universal Scaling Laws of Kerr Frequency Combs

Stéphane Coen,* and Miro Erkintalo

Physics Department, The University of Auckland, Private Bag 92019, Auckland 1142, New Zealand

*Corresponding author: s.coen@auckland.ac.nz

Compiled August 20, 2018

Using the known solutions of the Lugiato-Lefever equation, we derive universal trends of Kerr frequency combs. In particular, normalized properties of temporal cavity soliton solutions lead us to a simple analytic estimate of the maximum attainable bandwidth for given pump-resonator parameters. The result is validated via comparison with past experiments encompassing a diverse range of resonator configurations and parameters. © 2018 Optical Society of America

OCIS codes: 230.5750, 190.5530, 190.4380

Over the last few years, the generation of frequency combs in high-Q Kerr microresonators pumped by continuous-wave (cw) laser light has attracted considerable interest [1]. Despite this interest, the dependence of comb characteristics on the pump-resonator parameter-space remains largely unexplored, with little or no consensus existing on guidelines for Kerr comb optimization. This shortcoming originates from the computational complexity of traditional models, such as the coupled-mode equation model [2–4]. Approximate analytic solutions exist but the comb characteristics still cannot be inferred in closed form [5].

We have recently shown that Kerr frequency combs can be efficiently modeled using a generalized mean-field Lugiato-Lefever equation (LLE), and that they can be associated with the cavity soliton (CS) solutions of this equation [6]. Also Herr et al. have presented convincing experimental evidence in strong support of the CS hypothesis [7]. Here, we use the mean-field framework to identify universal trends in the dynamics and characteristics of Kerr frequency combs. Our objectives are two-fold: (i) we link the known solutions of the LLE into the Kerr comb context and (ii) use the solutions to derive *universal scaling laws* that allow comb bandwidths to be analytically estimated. Comparison with past experiments across a wide variety of resonator parameters and architectures shows good agreement with our results.

Our starting point is the normalized LLE [6, 8],

$$\frac{\partial E(t, \tau)}{\partial t} = \left[-1 + i(|E|^2 - \Delta) - i\eta \frac{\partial^2}{\partial \tau^2} \right] E + S. \quad (1)$$

Here t is the slow time describing the evolution of the intracavity electric field envelope $E(t, \tau)$ at the scale of the cavity photon lifetime while τ is a fast time defined in a reference frame traveling at the group velocity of light in the resonator. The terms on the right-hand side of Eq. (1) describe, respectively, cavity losses, Kerr nonlinearity, pump-cavity detuning, 2nd-order group-velocity dispersion (GVD), and external pumping. η is the sign of the GVD coefficient β_2 , and we assume here anomalous dispersion, $\eta = -1$. The normalization follows Ref. [8]: $t \rightarrow \alpha t / t_R$, $\tau \rightarrow \tau(2\alpha / |\beta_2| L)^{1/2}$, and $E \rightarrow E(\gamma L / \alpha)^{1/2}$. Here $t_R = \text{FSR}^{-1}$ is the cavity roundtrip time with FSR the free-spectral range, $\alpha = (\alpha_i L + \theta) / 2$ is the total round-trip loss parameter with α_i describing internal linear absorption and θ the input coupler power transmission

coefficient, and L is the resonator length. The nonlinearity coefficient $\gamma = 2\pi n_2 / (\lambda_p A_{\text{eff}})$ with n_2 the nonlinear refractive index, λ_p the pump wavelength, and A_{eff} the effective mode area. The solutions of Eq. (1) are governed by two normalized parameters: the pump strength $S = E_{\text{in}}(\gamma L \theta / \alpha^3)^{1/2}$, with E_{in} the cw pump amplitude in units of $W^{1/2}$, and the detuning $\Delta = \delta_0 / \alpha$, where δ_0 is the phase detuning of the pump from the closest cavity resonance. Note that Δ is formally identical to the ζ_0 parameter introduced in Ref. [7].

Under cw pumping, the simplest steady-state solutions of Eq. (1) are homogeneous ($\partial E / \partial \tau = 0$) and satisfy

$$X = Y^3 - 2\Delta Y^2 + (\Delta^2 + 1)Y, \quad (2)$$

where $X = |S|^2$ and $Y = |E|^2$ are the normalized pump and intracavity powers, respectively. Equation (2) is the well-known cubic equation of dispersive optical bistability [9]. At constant pump, it also describes the Kerr tilt of the cavity resonances as shown in Fig. 1(a) for $X = 10$ (black curve). Here X is large enough for $Y(\Delta)$ to be multivalued. The lower branch, existing for $\Delta > \Delta_{\dagger}$, is always stable [$\Delta_{\dagger} \simeq 3(X/4)^{1/3}$ for $X \gg 1$] while the intermediate branch (dotted black) is homogeneously unstable. The left side of the resonance, including the upper branch of the multivalued region, exhibits modulation instability (MI) for intracavity powers above the threshold $Y > 1$ [9], or equivalently for detunings $\Delta > \Delta_{\text{MI}} = 1 - \sqrt{X - 1}$ (dashed black). Accordingly $X = 1$ is the absolute MI threshold, also referred to as the hyperparametric threshold in the comb literature [1–3].

MI leads to patterned solutions [9] and the green curve in Fig. 1(a) represents the peak power of a range of such solutions ($X = 10$ as above). They are steady-state periodic solutions of Eq. (1) and have been obtained with a Newton solver and a continuation method [6]. Here the MI frequency is set to the most unstable one at threshold. For the point highlighted by the green cross, we have also plotted in Figs. 1(b)–(c) the corresponding temporal and spectral intensity profiles. As can be seen, an MI solution corresponds in the spectral domain to a frequency comb, but resonators are typically long enough to fit multiple periods of the pattern, so the comb modes would be separated by multiple FSRs. For larger Δ , the MI branch becomes unstable (dotted green), and split-step simulations of Eq. (1) reveal a transition to chaotic combs whose broadband components are separated by a single FSR, as also

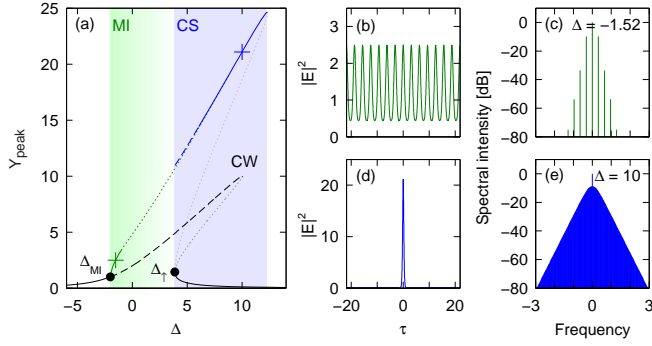


Fig. 1. (Color online) (a) Intracavity peak power versus detuning for the cw (black), MI (green), and CS (blue) branches. Dashed and dotted lines indicate unstable solutions as described in the text. The temporal and spectral intensity profiles of particular MI and CS solutions (crosses) are illustrated in (b,c) and (d,e), respectively.

observed from the coupled-mode equation model [4].

CSs constitute the last class of steady-state solutions of Eq. (1) [6, 8]. Their peak power, obtained as for the MI branch, completes Fig. 1(a) [blue curve]. In the time domain, CSs are localized pulses sitting atop a cw background and, due to resonator periodic boundary conditions, correspond to a frequency comb in the spectral domain [6]. A typical solution (blue cross) is illustrated in Figs. 1(d)–(e). Here the comb separation is a single FSR as there is only one CS in the cavity. The CS background matches with the lower state homogeneous solution, as it is the only stable cw solution, hence CSs only exist above the up-switching point, $\Delta > \Delta_{\uparrow}$. It is also found that CS existence is limited to a maximum detuning of about $\pi^2 X/8$ [10]. The lower part of the CS branch is always unstable (dotted blue). On the upper branch, CSs go through a Hopf bifurcation for lower detunings (dashed blue). Here CSs are oscillating (breathing) over multiple round-trips [10–12]. More complex chaotic regimes also exist in this region [12].

In the context of Kerr frequency combs, important conclusions emerge from the (co)existence of the cw, MI, and CS solutions represented in Fig. 1(a). CSs are the preferred solutions for combs because, in comparison to MI, they are stable over a wider parameter range and their peak power is higher, leading to broader spectral bandwidths. However, CSs cannot spontaneously emerge from an initial cw background as stable CS solutions are disconnected from the cw branch [8]. Moreover, to exploit thermal self-locking, the resonance is approached from the high frequency side [from the left in Fig. 1(a)]. Combined with the fact that Δ_{MI} is *always* smaller than Δ_{\uparrow} , it implies that *MI will always occur first*. The onset of MI can therefore be associated with the “primary combs” described in other works [2]. The MI branch extends into the CS branch, but unstable (chaotic or otherwise) MI and CS states lie in between the onset of MI and the desirable stable CSs. Although beyond the scope of this Letter, preliminary simulations show that a chaotic MI state can condensate into a set of CSs with appropriate ramping of Δ . Note that the chain stable $\text{MI} \rightarrow \text{chaotic MI} \rightarrow \text{stable CSs}$ as implied by Fig. 1(a) is precisely that observed in recent experiments [7].

In the CS regime, the comb bandwidth is determined by the temporal duration of the CS. To gain some general in-

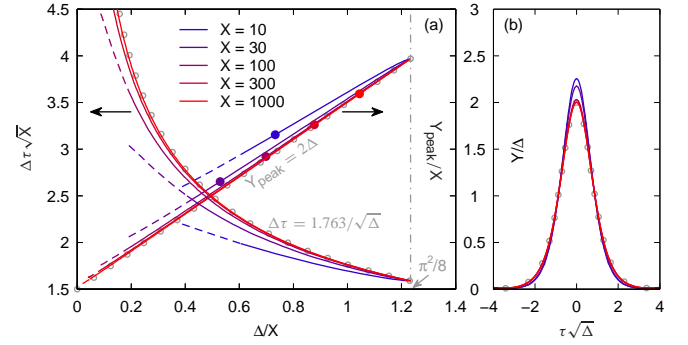


Fig. 2. (Color online) (a) Normalized CS duration (left axis) and peak power (right axis) versus Δ/X for various pump levels (dashed: oscillatory CSs; other unstable CSs are omitted for clarity). (b) Examples of numerical CS temporal intensity profiles for parameters corresponding to the dots in (a). In both panels, the numerical results are compared with analytic approximations (grey circles).

sights, we have calculated CS characteristics across a wide range of parameters. In Fig. 2(a), we plot the full-width at half-maximum (FWHM) $\Delta\tau$ of the CS solution (left axis) and its peak power Y_{peak} (right axis) as a function of cavity detuning for several values of X . Note how we have normalized all axes based on X to reveal universal CS trends. We see that the CS peak power increases linearly with detuning, with a slope approaching two for increasing values of X , i.e., $Y_{\text{peak}} \simeq 2\Delta$. As the peak power increases, the CS duration decreases and approaches $\Delta\tau \simeq 1.763/\sqrt{\Delta}$ for $X \gg 1$. In Fig. 2(b) we also show normalized temporal intensity profiles of selected solutions [dots in Fig. 2(a)] superimposed with a sech^2 pulse with peak power and duration as derived above. Agreement is excellent for all parameters, implying that CSs can be approximated as $E_{\text{CS}} \simeq \sqrt{2\Delta} \text{sech}(\sqrt{\Delta}\tau)$. It is worth noting that this expression is an exact analytical solution of the normalized LLE (1) for a pulsed pump identical to the soliton, $S(\tau) = E_{\text{CS}}$, and is also found by perturbation theory as the fixed point of (1) [7, 13], as well as in the solution derived by Barashenkov and Smirnov with $X = \Delta \gg 1$ [5, 10].

Considering E_{CS} to be a good approximation of the intracavity field allows us to derive a simple estimate for the comb bandwidth obtainable for given pump-resonator parameters. Specifically, assuming on-resonance pumping ($\Delta = X$) and critical coupling ($\alpha = \theta$), and transforming into physical units, we get the following simple theoretical estimate for the 3-dB comb bandwidth,

$$\Delta f_{\text{theo}} = \frac{0.315}{1.763} \sqrt{\frac{2\gamma P_{\text{in}} Q \lambda_p \text{FSR}}{\pi c |\beta_2|}} = \frac{0.315}{1.763} \sqrt{\frac{2\gamma P_{\text{in}} \mathcal{F}}{\pi |\beta_2|}}, \quad (3)$$

with $P_{\text{in}} = |E_{\text{in}}|^2$ the pump power, Q the quality factor of the cavity, and c the speed of light. Eq. (3) also reveals the relevance of the various parameters. Recalling that the cavity finesse $\mathcal{F} = \pi/\alpha = Q\lambda_p \text{FSR}/c$, it is clear that the suitability of a given resonator for broadband comb generation is determined solely by its finesse (or losses), nonlinearity, and GVD coefficient, and is independent of its FSR. Note that MI generally follows trends similar to CSs such that Eq. (3) is qualitatively correct irrespective of the operation regime.

Table 1. Comparison of experimental 3-dB comb bandwidths (Δf_{exp}) with analytical predictions (Δf_{theo}).

Ref.	γ [$\text{W}^{-1}\text{km}^{-1}$]	P_{in} [mW]	λ_p [nm]	Q	FSR [GHz]	\mathcal{F}	β_2 [$\text{ps}^2\text{km}^{-1}$]	Δf_{exp} [THz]	Δf_{theo} [THz]
[7]	0.405	24	1553	$400 \cdot 10^6$	35.2	$73 \cdot 10^3$	-5.9	1.6	1.59
[14]	15	160	1550	$100 \cdot 10^6$	882	$460 \cdot 10^3$	-6.3	31	36.4
[15]	800	2000	1562	$3 \cdot 10^5$	226	350	-47	10	15.6
[16]	0.032	55.6	1560	$1.90 \cdot 10^9$	18.2	$180 \cdot 10^3$	-13	0.6	0.71
[17]	25	1000	1550	$270 \cdot 10^6$	850	$1.2 \cdot 10^6$	-4.0	40	388

The validity of Eq. (3) has been checked by comparing its predictions against experimental comb bandwidths for a number of references, as summarized in Table 1, with all relevant experimental parameters also listed. Aside from the comb reported in [17], agreement is good throughout, with discrepancies attributed to inaccuracies in experimental parameters, difficulties in estimating the bandwidths of highly-structured experimental combs, as well as approximations implicit in Eq. (3). Note in particular how the comparatively low finesse and high GVD of the resonator used in [15] is offset by the large nonlinearity (γP_{in} product). The large deviation between the estimated and experimental bandwidths for [17] stems from the LLE (1) and Eq. (3) not taking into account higher-order dispersion. This approximation becomes inaccurate for comb spectra extending into the normal GVD regime, and results in significant over-estimation of the bandwidth. We can mitigate this issue by recalling that CSs perturbed by higher-order dispersion emit dispersive waves (DW) into the normal GVD regime [6, 18, 19]. Assuming that the 3rd-order GVD coefficient β_3 is the dominant contribution, the DW frequency shift can be written as $\Delta f_{\text{DW}} = 3|\beta_2|/(2\pi\beta_3)$. Because the generated DWs are linear (they reside in a spectral region not supporting solitons), no significant spectral broadening is expected beyond their spectral shift. We can thus interpret $\Delta f_{\text{lim}} = 2\Delta f_{\text{DW}}$ as being an *upper limit* of the full-width bandwidth of a Kerr comb. Interestingly, while Eq. (3) suggests that low GVD is beneficial for broadband combs, the full-width limit bandwidth Δf_{lim} is in this case constrained to a lower value. It is only a low dispersion slope β_3 (i.e., flat dispersion) that can lift this limit. These trends are illustrated in Fig. 3 where we plot the bandwidths estimated from Eq. (3) as a function of β_2 for various values of the product $\gamma P_{\text{in}} \mathcal{F}$ (solid lines) as well as the full-width upper limit Δf_{lim} (dotted line), assuming here $\beta_3 = 0.1 \text{ ps}^3/\text{km}$. In Fig. 3 we also

show the experimental (green dots) and theoretical [Eq. (3); black diamonds] bandwidths extracted from Table 1. Note in particular how the comb bandwidth observed in [17], overestimated by Eq. (3), falls on the theoretical upper limit.

To conclude, we have analyzed the solutions of a dimensionless mean-field equation from the Kerr comb perspective. By identifying universal trends in the solutions we have derived universal scaling laws linking experimental pump-resonator parameters to the obtainable comb bandwidth.

We acknowledge support from the Marsden Fund (Royal Society of New Zealand) and useful discussions with T. Herr.

References

1. T. J. Kippenberg, R. Holzwarth, and S. A. Diddams, *Science* **332**, 555 (2011).
2. Y. K. Chembo and N. Yu, *Phys. Rev. A* **82**, 033801 (2010).
3. A. B. Matsko, A. A. Savchenkov, V. S. Ilchenko, D. Seidel, and L. Maleki, *Phys. Rev. A* **85**, 023830 (2012).
4. A. B. Matsko, W. Liang, A. A. Savchenkov, and L. Maleki, *Opt. Lett.* **38**, 525 (2013).
5. A. B. Matsko, A. A. Savchenkov, W. Liang, V. S. Ilchenko, D. Seidel, and L. Maleki, *Opt. Lett.* **36**, 2845 (2011).
6. S. Coen, H. G. Randle, T. Sylvestre, and M. Erkintalo, *Opt. Lett.* **38**, 37 (2013).
7. T. Herr, V. Brasch, M. L. Gorodetsky, T. J. Kippenberg, arXiv:1211.0733.
8. F. Leo, S. Coen, P. Kockaert, S.-P. Gorza, Ph. Emplit, and M. Haelterman, *Nat. Photon.* **4**, 471 (2010).
9. M. Haelterman, S. Trillo, and S. Wabnitz, *Opt. Comm.* **91**, 401 (1992).
10. I. V. Barashenkov and Yu. S. Smirnov, *Phys. Rev. A* **54**, 5707 (1996).
11. A. B. Matsko, A. A. Savchenkov, and L. Maleki, *Opt. Lett.* **37**, 4856 (2012).
12. F. Leo, L. Gelens, Ph. Emplit, M. Haelterman, and S. Coen, accepted in *Opt. Express* (2013).
13. S. Wabnitz, *Opt. Lett.* **18**, 601 (1993).
14. P. Del’Haye, A. Schliesser, O. Arcizet, T. Wilken, R. Holzwarth, and T. J. Kippenberg, *Nature* **450**, 1214 (2007).
15. Y. Okawachi, K. Saha, J. S. Levy, Y. H. Wen, M. Lipson, and A. L. Gaeta, *Opt. Lett.* **36**, 3398 (2011).
16. I. S. Grudin, L. Baumgartel, and N. Yu, *Opt. Express* **20**, 6604 (2012).
17. P. Del’Haye, T. Herr, E. Gavartin, M. L. Gorodetsky, R. Holzwarth, and T. J. Kippenberg, *Phys. Rev. Lett.* **107**, 063901 (2011).
18. M. Erkintalo, Y. Q. Xu, S. G. Murdoch, J. M. Dudley, and G. Genty, *Phys. Rev. Lett.* **109**, 223904 (2012).
19. F. Leo, A. Mussot, P. Kockaert, Ph. Emplit, M. Haelterman, and M. Taki, *Phys. Rev. Lett.* **110**, 104103 (2013).

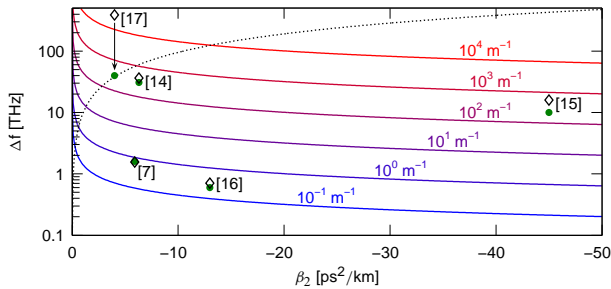


Fig. 3. (Color online) Theoretical Kerr comb bandwidth calculated from Eq. (3) versus 2nd-order GVD for varying values of $\gamma P_{\text{in}} \mathcal{F}$ (solid lines) and upper limit (dotted line). The black diamonds are the theoretical estimates for the References listed in Table 1 with the corresponding experimental bandwidths shown as green dots.

References with titles

References

1. T. J. Kippenberg, R. Holzwarth, and S. A. Diddams, "Microresonator-based optical frequency combs," *Science* **332**, 555–559 (2011).
2. Y. K. Chembo and N. Yu, "Modal expansion approach to optical-frequency-comb generation with monolithic whispering-gallery-mode resonators," *Phys. Rev. A* **82**, 033801/1–18 (2010).
3. A. B. Matsko, A. A. Savchenkov, V. S. Ilchenko, D. Seidel, and L. Maleki, "Hard and soft excitation regimes of Kerr frequency combs," *Phys. Rev. A* **85**, 023830/1–5 (2012).
4. A. B. Matsko, W. Liang, A. A. Savchenkov, and L. Maleki, "Chaotic dynamics of frequency combs generated with continuously pumped nonlinear microresonators," *Opt. Lett.* **38**, 525–527 (2013).
5. A. B. Matsko, A. A. Savchenkov, W. Liang, V. S. Ilchenko, D. Seidel, and L. Maleki, "Mode-locked Kerr frequency combs," *Opt. Lett.* **36**, 2845–2847 (2011).
6. S. Coen, H. G. Randle, T. Sylvestre, and M. Erkintalo, "Modeling of octave-spanning Kerr frequency combs using a generalized mean-field LugiatoLefever model," *Opt. Lett.* **38**, 37–39 (2013).
7. T. Herr, V. Brasch, M. L. Gorodetsky, T. J. Kippenberg, "Soliton mode-locking in optical microresonators," arXiv:1211.0733.
8. F. Leo, S. Coen, P. Kockaert, S.-P. Gorza, Ph. Emplit, and M. Haelterman, "Temporal cavity solitons in one-dimensional Kerr media as bits in an all-optical buffer," *Nat. Photon.* **4**, 471–476 (2010).
9. M. Haelterman, S. Trillo, and S. Wabnitz, "Dissipative modulation instability in a nonlinear dispersive ring cavity," *Opt. Comm.* **91**, 401–407 (1992).
10. I. V. Barashenkov and Yu. S. Smirnov, "Existence and stability chart for the ac-driven, damped nonlinear Schrödinger solitons," *Phys. Rev. A* **54**, 5707–5725 (1996).
11. A. B. Matsko, A. A. Savchenkov, and L. Maleki, "On excitation of breather solitons in an optical microresonator," *Opt. Lett.* **37**, 4856–4858 (2012).
12. F. Leo, L. Gelens, Ph. Emplit, M. Haelterman, and S. Coen, "Dynamics of one-dimensional Kerr cavity solitons," accepted in *Opt. Express* (2013).
13. S. Wabnitz, "Suppression of interactions in a phase-locked soliton optical memory," *Opt. Lett.* **18**, 601–603 (1993).
14. P. Del'Haye, A. Schliesser, O. Arcizet, T. Wilken, R. Holzwarth, and T. J. Kippenberg, "Optical frequency comb generation from a monolithic microresonator," *Nature* **450**, 1214–1217 (2007).
15. Y. Okawachi, K. Saha, J. S. Levy, Y. H. Wen, M. Lipson, and A. L. Gaeta, "Octave-spanning frequency comb generation in a silicon nitride chip," *Opt. Lett.* **36**, 3398–3400 (2011).
16. I. S. Grudin, L. Baumgartel, and N. Yu, "Frequency comb from a microresonator with engineered spectrum," *Opt. Express* **20**, 6604–6609 (2012).
17. P. Del'Haye, T. Herr, E. Gavartin, M. L. Gorodetsky, R. Holzwarth, and T. J. Kippenberg, "Octave spanning tunable frequency comb from a microresonator," *Phys. Rev. Lett.* **107**, 063901/1–4 (2011).
18. M. Erkintalo, Y. Q. Xu, S. G. Murdoch, J. M. Dudley, and G. Genty, "Cascaded phase matching and nonlinear symmetry breaking in fiber frequency combs," *Phys. Rev. Lett.* **109**, 223904/1–5 (2012).
19. F. Leo, A. Mussot, P. Kockaert, Ph. Emplit, M. Haelterman, and M. Taki, "Nonlinear symmetry breaking induced by third-order dispersion in optical fiber cavities," *Phys. Rev. Lett.* **110**, 104103/1–5 (2013).